DEPTH-AVERAGED FLOW RECONSTRUCTION IN AN EXTREMELY SHALLOW ESTUARY

MAHDI RAZAZ[1], KIYOSI KAWANISI[2], IOAN NISTOR[3], LEN ZEDEL[4]

1 Department of Physical Oceanography, Memorial University of Newfoundland, St. John's, NF, Canada, mrazaz@mun.ca

2 Department of Civil and Environmental Engineering, Graduate School of Engineering, Hiroshima University, Higashi-Hiroshima, Japan, kiyosi@hiroshima-u.ac.jp

3 Department of Civil Engineering, Faculty of Engineering, University of Ottawa, Canada, inistor@uottawa.ca

4 Department of Physical Oceanography, Memorial University of Newfoundland, St. John's, NF, Canada, zedel@mun.ca

ABSTRACT

Tomographic techniques have been used to probe ocean currents and temperature for nearly six decades. However, application of such techniques is strongly restricted in the acoustically shallow waters mainly due to the interaction of sound with the stochastic boundaries. The acoustic tomography technique relies on stringent measurements of the time it takes sound pulses to propagate from transmitter to a receiver. To fulfill this requirement in rivers and estuaries, high sound frequencies – above 10 kHz – along with an accurate clock must be used to indicate, keep, and co-ordinate time. Fluvial Acoustic Tomography (FAT) system is a technique/instrument that is able to emit pulses with central frequencies up to 57 kHz and its 10 MHz accurate GPS clock allows accurate measurements of time and frequency. One fascinating application of FAT is 2D flow pattern visualization in shallow waters. Herein, we present an example application of an array of FAT in an extremely shallow tidal channel in conjunction with numerical inversion schemes. Although the salt-wedge intrusion had strong effect on sound propagation patterns which led to a multitude of arrival times, reconstructed flow patterns compared favorably with underway moving-boat ADCP data.

KEWORDS: Shallow-water tomography, estuary, flow visualization, inverse analysis.

1   INTRODUCTION

Ocean acoustic tomography (OAT) is a travel-time technique that can be used to map the sound-speed field in a given region of water. OAT and other travel-time tomography techniques use the time-of-flight for a signal sent between a sender and receiver to infer information about the conditions of the region under study. Traditionally, application of tomographic techniques was strictly limited to deep waters and despite clear advantages of OAT over other monitoring techniques; it could not be used in bays and estuaries primarily due to the interaction of sound with the stochastic boundaries.

The shallow acoustic tomography technique has been under development for a number of years at Hiroshima University. Efforts of Kaneko et al. (1994), Kawanisi et al. (2010) and Razaz et al. (2013) resulted in a new travel-time tomography technique/system that makes it possible to measure the sound arrival times in extremely shallow waters. The new system is called Fluvial Acoustic Tomography (FAT) and is designed for continuous measurement of the cross-sectional average velocities using higher frequencies in the range of 10-57 kHz emitted from omnidirectional transducers. To surmount some of the difficulties associated with acoustic propagation in shallow waters and to achieve accurate measurements, the carrier signal is modulated with an M-sequence (Simon et al., 1985). It is worth to mention that in the present context, "shallow water" term describes a body of water with depth in the range of 0.3 m to maximum 10 m in which sound propagates over a certain distance by repeated reflections from both the water surface and bottom. The FAT ability to reconstruct flow velocity magnitude and direction with only two crossing paths has already resulted in a wealth of applications, for instance, measurement of dam flush in a mountainous river and measurement of flow in a shallow estuary. A fascinating application of FAT is, however, deploying an array of acoustic stations and translating the collected data into

depth-averaged flow velocity distribution pattern using inversion schemes. Razaz et al. (2016) positioned an array of eight FAT's in perimeters of a shallow mountainous river for twelve weeks and used the collected data to map the depth-averaged flow pattern. The survey site was characterized with extremely shallow flow depth, i.e. about 0.3 m near the banks where transducers were installed and a maximum depth of 3.5 m at the deepest part of the river, and absence of salinity intrusion and unidirectional flow. The tomographically derived 2D velocity field showed excellent agreement with two stationary ADCP data.

Contained herein are the results of reciprocal transmission among 8 acoustic stations in the upper reach of a tidally dominated channel. The survey performed for about 9 hours of 17 December 2013 and includes one flood and ebb of a semidiurnal tide. The surveyed zone is characterized by unsteady and complex flow distribution pattern generated by the frequent intrusion of saline water, the occasional opening of sluice gates that control freshwater diversion, and irregular bathymetry.

2   SURVEY SITE AND DATA ACQUISITION

The Ota River is a network of tide-dominated river branches that flow through Hiroshima City, Japan. As shown in Figure 1(a), the mainstream bifurcates into two main branches nearly 9 km before discharging into the Hiroshima Bay; the westernmost branch is called Ota Diversion Channel. Arrays of sluice gates regulate the amount of freshwater inflow to each branch. During normal operation, only 1/3 of the Gion Sluice Gates are open. The Gion Sluice Gates open during flood events affecting the channel bed composition. Channel bed in downstream of the gates is mainly comprised of loosely settled fine sand, and some gravel and boulder close to the banks.

The FAT measurement campaign was carried out between 6:00-15:00 JST on 17 December 2013. As shown in Figure 1b, an array of FAT comprised of 8 acoustic stations was installed along the shallow banks of the channel in an area approximately 190 m long by 130 m wide. Such arrangement of transducers would normally allow simultaneous, reciprocal sound transmissions along $8(8-1)/2 = 28$ ay paths in open waters. However, the sound transmission was inhibited along 12 ray paths which are parallel to the banks and therefore in total simultaneous reciprocal transmissions were conducted along 16 ray paths. Each acoustic stations was comprised of a Neptune Sonar T257 broadband monostatic transducer with a source level of 197 dB re 1 mPa mounted on bottom pods with three lead feet to keep transducers 0.2 m above the bed level. Every 75 sec, a signal with 30 kHz central frequency and an effective bandwidth of 20-35 kHz was generated simultaneously from each source and received by the other 7 stations. Signals were modulated by an M-sequence of order 9 to increase the processing gain by about 27.1 dB. M-sequence is a type of pseudorandom signals by which the phase shift of in the carrier is generated with irregular time intervals.
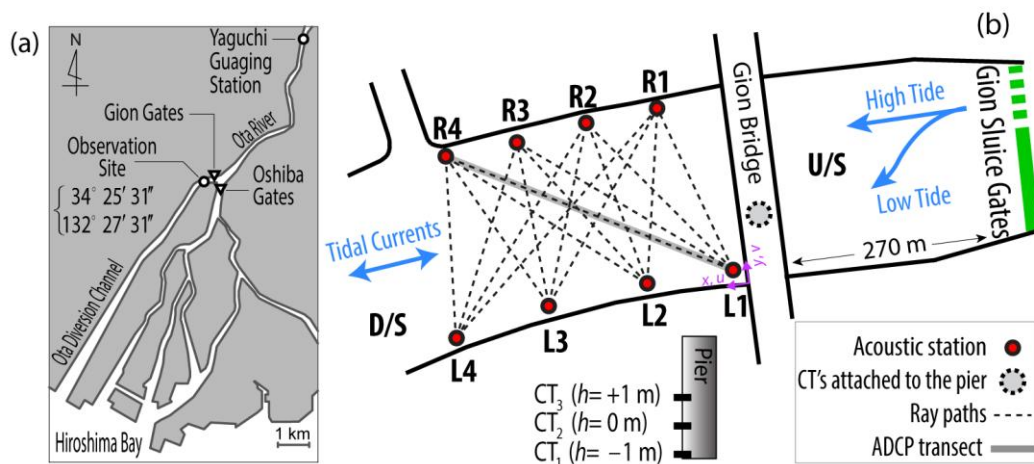

Figure 1. (a) Schematic map of the Ota River network, and (b) survey site plan with the location of 8 acoustic stations as well as the ADCP round-trip path and CT's attached to the Gion Bridge pier.

Simultaneous to the FAT measurements, round trips of moving-boat ADCP were performed along R4-L1 transect to provide reference velocity data. Water velocities were acquired through the pulse-coherent mode of a Teledyne RDI 1200 kHz Workhorse Monitor ADCP. The velocity bin size was set to 0.02 m and measured velocities were 7-ping-averaged. Blank distance was set to 0.10 m. All the data were referenced to the ADCP bottom tracking. Drift in the bottom tracking due to moving bed effects or compass error was not significant. Each transect began from or ended near the bank. During each transect, the boat speed was maintained approximately 0.25 m/s and, as a result, the boat travel time was about 15
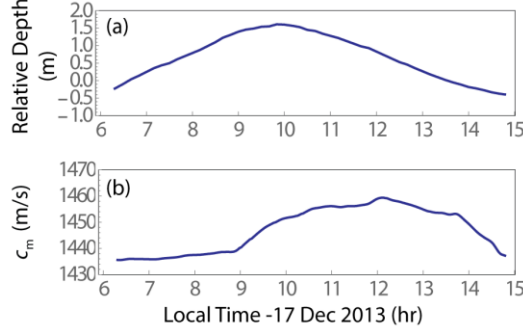
Figure 2. (a) Relative depth of the channel at the survey site, and (b) sound propagation speed approximated from CT readings.

minutes. A wire across the river was used as a lead to make similar paths; however tidally induced depth variations somewhat affected the transect length.

Variations of salinity and temperature during the observation period was measured using 3 conductivity-temperature (CT) sensors attached to the pier of Gion Bridge located 40 m away from the southern bank (Figure 1b). Figure 2 shows the relative depth and the sound speed determined from CT sensors using the equation proposed by Medwin (1975)

$$c = 1449.2 + 4.6T - 0.055T^2 + 2.9 \times 10^{-4}T^3 + (1.34 - 0.01T)(S - 35) + 0.016D \qquad (1)$$

with the limits of $0 \le T \le 35\ °C$ and $0 \le S \le 45$. In the equation above D denotes the depth in meter, T temperature, and S salinity.

3   METHODOLOGY

Using the geometric optics approximation, the travel time along a ray path, Γ_i, in the presence of a current $\mathbf{u}(x, y)$ can be expressed as

$$t_i^{\pm} = \int_{\Gamma_i^{\pm}} \frac{ds}{C_m + \delta C(x, y) \pm \mathbf{u}(x, y).\mathbf{n}_i} \qquad (2)$$

where ds and C_m are the increment of length and average sound speed along the ray path, respectively, δC is the sound speed perturbation relative to C_m, $\mathbf{n}_i$ is a unit vector tangent to the ray path i, while the sign $\pm$ depends on the direction of sound propagation. The travel times in opposite directions $t_i^{\pm}$ differ due to the effect of the current's speed. Given that $\delta C \ll C_m, \mathbf{u}(x, y).\mathbf{n} \ll C_m$, and assuming that the reciprocal sound rays travel along the same paths between the two acoustic stations, the travel time difference, Δt_i, can be then expressed by

$$\Delta t_i = \frac{1}{2}(t_i^+ - t_i^-) = -\int_{\Gamma_i} \frac{\mathbf{u}(x, y).\mathbf{n}_i}{C_m^2} ds \qquad (3)$$

Regarding the shallowness of the river, when deriving Equation (4), it is assumed that the length along the curve is roughly equal to the horizontal distance ($\Gamma_i^{\pm} = \Gamma_i$) between the source and receive. Equation (4) constitutes the forward problem in which the velocity field $\mathbf{u}(x, y)$ is used to predict a finite dataset, Δt_i.

Acoustic tomography is, however, a type of inverse problem in which the information, Δt_i, brought by the sound propagation through the flow field of interest is used to infer the field velocity, $\mathbf{u}(x, y)$. To proceed, the continuous velocity field is parameterized with a finite number of discrete parameters. As such, a truncated Fourier series is chosen to represent the horizontal state of streamlines. In the Cartesian coordinate system, a stream function Ψ defined at any time t and any location (x, y) can be written as

$$\Psi(x, y, t) = c_0 x + d_0 y + \sum_{k=0}^{n_x} \sum_{\ell=0}^{n_y} \left\{ C_{kl}(t) \cos\left[2\pi\left(\frac{kx}{L_x} + \frac{\ell y}{L_y}\right)\right] + D_{kl}(t) \sin\left[2\pi\left(\frac{kx}{L_x} + \frac{\ell y}{L_y}\right)\right] \right\} \qquad (4)$$

where, n_x and n_y are the number of Fourier coefficients along the x- and y-axis, respectively. Similarly, L_x and L_y are the side lengths of the computational domain which are taken twice as long as those of the physical domain to avoid

3

enforcing periodicity effects; c_0, d_0, C_{kl}, and D_{kl} are desired model parameters. For both directions, the number of Fourier series coefficients is taken as $n_x = n_y = n = 3$ to ensure a trade-off between the number of unknowns in the inverse problem and the resolvable curvature of the flow currents. Reordering the locale dependence and indexing Equation (4) leads to

$$\Psi\left(x, y, t\right) = c_0 x + d_0 y + \sum_{j=1}^{(n+1)^2} m_j(t) X_j\left(x, y\right) \tag{5}$$

According to the projection slice theorem postulated by Munk et al. (1995), the non-rotational component of the flow field induced by tides and/or by the bottom morphology have no influence on the tomography results expressed by the stream function. And, therefore, in a horizontal plane, the velocity field $\mathbf{u}$ is set as $\mathbf{u} = \nabla \times \Psi$. In the Cartesian coordinates, this is equivalent to $u = \partial\Psi/\partial y$ and $v = -\partial\Psi/\partial x$. Equation (3) can be rewritten in the form of

$$\frac{\Delta t_i}{2} C_m^2 = \sum_{j=1}^{(n+1)^2} m_j \left(\int_{\Gamma_i} \frac{\partial X_j}{\partial y} dx - \int_{\Gamma_i} \frac{\partial X_j}{\partial x} dy \right) \tag{6}$$

In matrix notation, Equation (6) can be written in form of a general inverse problem as

$$\mathbf{d} = \mathbf{Gm} \tag{7}$$

Here, matrix $\mathbf{d}$ contains the observed data, and matrix $\mathbf{G}$ ensures the dependence of the i-th model parameter to the j-th datum. One needs to obtain the estimates $\hat{\mathbf{m}}$ of the true model parameters $\mathbf{m}$.

The approach proposed here for reconstructing the flow field does not take into account the irregularities or variations in depth and treats the target zone with a uniform depth equivalent to the average depth of the survey site.

4   RESULTS AND DISCUSSION

4.1 ADCP Measurements

In order to evaluate the velocities derived from solving the inverse problem, ADCP data had to be post processed to establish reference mean velocity data. The first correction needs to be done is the sound speed. ADCP approximate sound speed and based on a constant salinity and temperature readings. It is, therefore, necessary to account for the vertical
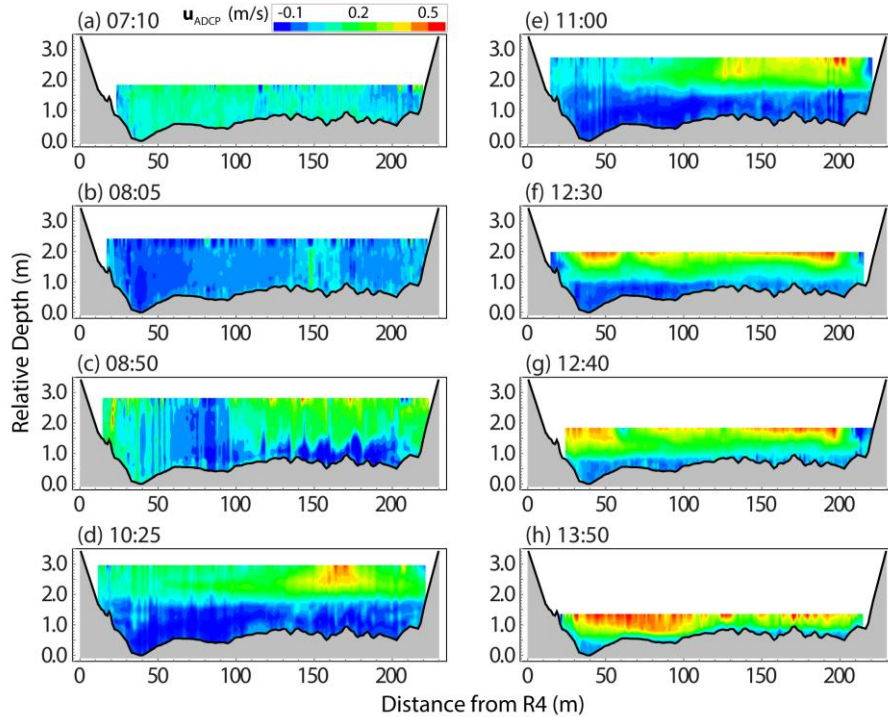

Figure 3. Typical moving-boat ADCP readings along the R4-L1 path. Relative depth is measured with respect to the deepest point of the transect.

gradients of sound speed in stratified flows. Assuming that the horizontal salinity and temperature gradients are negligible in the survey site, CT readings were used to correct the depths and velocity data collected by the ADCP. After implementing sound speed corrections, in order to reduce dispersion induced by turbulence, density stratification, as well as Doppler noise linked to the ADCP technology, the inverse distance weighting (IDW) method was applied to the velocity data. ADCP vertical velocity profiles deviated from the logarithmic profile. Hence, the authors used a different strategy and used the extrapolation of the top 5 good bins to produce data for the top layer. This method extrapolates data in a straight line to the surface. For the missing layer caused by the side-lobe effect, the bins present in the lower 20% of the depth were used to determine a power fit. This fit was forced to pass through zero at the bed. Typical transects shown in Figure 3 demonstrate the complex and highly variable nature of flow structure in the survey field.

4.2 FAT Measurements

To demonstrate typical examples of variation of arrival time during the survey period, time-varying correlation diagrams for reciprocal sound transmission between stations R4 and L1, and R4 and L4 are shown in Figure 4. Despite the presence of strong vertical salinity stratification along the path, the irregular bottom shape, and a noticeable signal attenuation due to numerous interactions with water surface and the bottom, the arrival pattern for the path R4-L1 is relatively stable. However, the effect of strong salinity gradient caused by salt wedge intrusion can be seen clearly along the R4-L4 path. It seems that during tide reversal period at high tide two sound conduits were formed by the two layers of the flow –cold freshwater on top, and warm saline water at the bottom – and the sound is trapped inside each conduit. In Figure 4(d) the early arrivals can be attributed to the sound rays trapped inside the salt wedge and the ones trapped inside freshwater arrived a few micro seconds later as the sound propagates slower in the cold freshwater. Sound entrapment issue is discussed comprehensively in (Razaz et al., 2013). The overall trend of arrival time corresponds to the sound propagation speed variations caused by tidal currents.
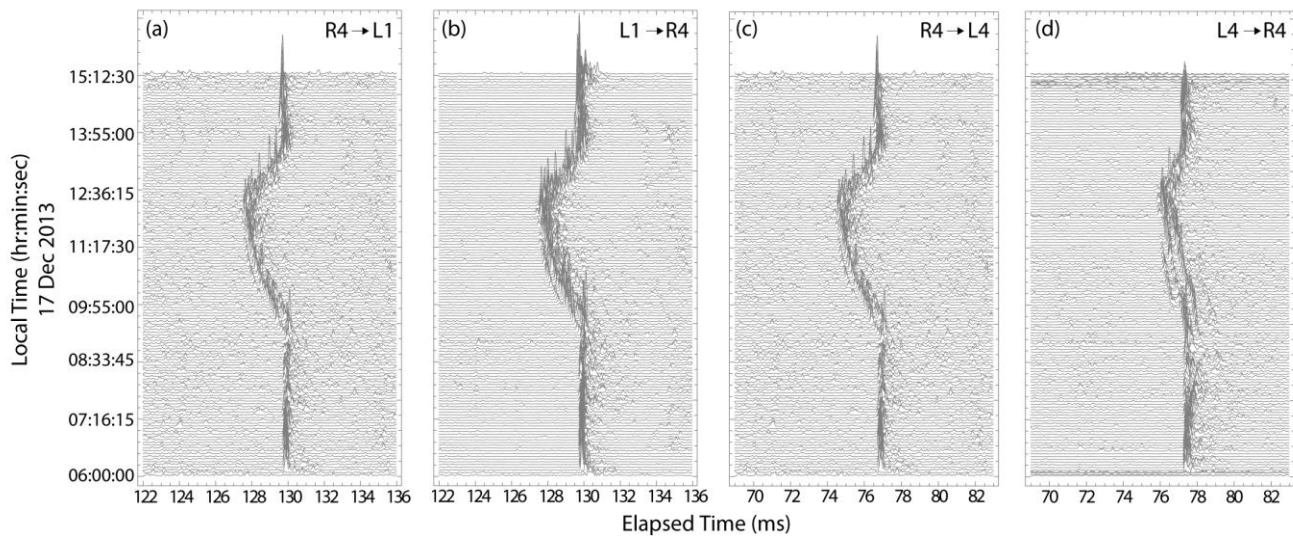

Figure 4. Stack diagram of the correlated signals for the entire transmission period for the R1–L4 and R4-L4 reciprocal transmission paths.

4.3 Depth-Averaged Flow Velocity Fields

To reconstruct the flow field distribution using the inversion scheme described in the previous section, the measured $\frac{1}{2}C_m^2\langle Dt_i\rangle$ values served as input data, $\mathbf{d}$, while truncated Fourier series coefficients as well as c_0, d_0 were estimated by applying the zeroth-order Tikhonov regularization method. The angle brackets stand for low-pass filtering. Figure 9 shows typical depth-averaged flow distribution inside the tomography domain. Flow distribution pattern is very unsteady and complex in the survey site because it the location where tidal current meets the freshwater diverted asymmetrically from the Gion Sluice Gates. Bathymetry irregularities also contribute to the complexity of the flow pattern particularly during energetic tide reversal periods through which flow depth is less than 0.5 m. Despite the flow pattern changes were rapid, the spatial "snapshot" patterns derived from tomographic measurements, shown in Figure 5, compare favorably with the underway ADCP measurements, Figure 3.

Figure 6 compares the section-averaged velocities obtained from ADCP against those derived from tomographic measurements. This figure implies that there is a good agreement between the two techniques most the time despite the fundamental differences between the two techniques. However, the inversion results deviates significantly from ADCP

5

measurements between 9:30-11:00, which can be attributed to high-water slack and ebb initiation. Razaz et al. (2013) reported the susceptibility of shallow acoustic tomography, in particular FAT, to strong vertical stratification state induced by saltwater intrusion. That is, as a result of strong vertical stratification two distinct wave guides are formed, and depending on the vertical position of the source and receive sound can be trapped in either of them. As the upper layer consists freshwater, sound speed is less than that in the lower layer, thus, if the sound is trapped in the upper wave guide the current speeds will be overestimated. If the waveguide in which the sound is trapped is considerably thinner than the other one, flow direction will also be opposite of what expected. Through this observation the two waveguides with opposite directions can be seen clearly in Figure 3(d).
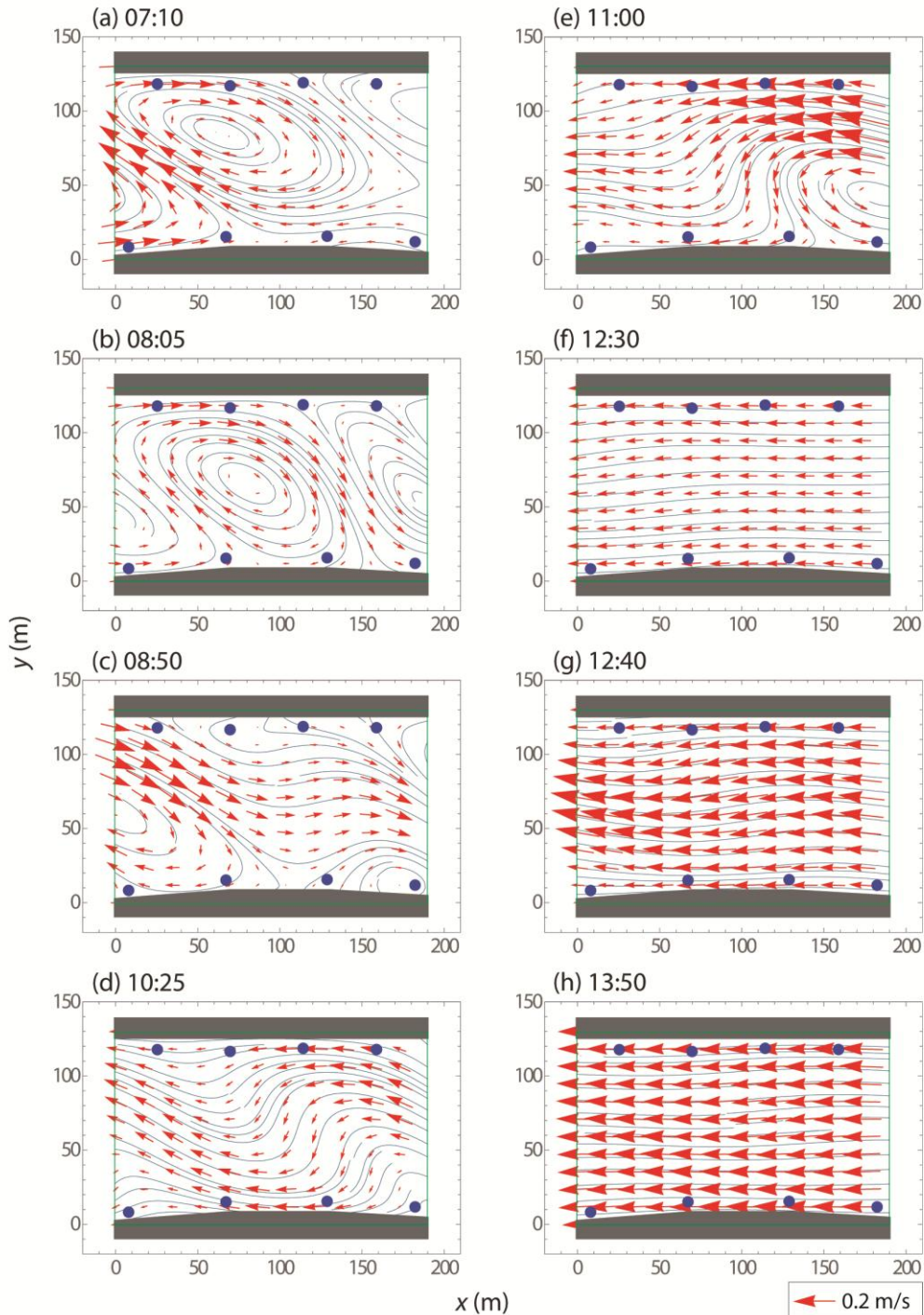

Figure 5. Typical reconstructed 2D velocity fields. Location of acoustic stations and stationary ADCPs are denoted by filled circles while the green rectangular lines delineate the computation domain.

5   CONCLUSIONS

An array of 8 fluvial acoustic tomography systems was positioned along the banks of Ota Diversion Channel in order to estimate the depth-averaged velocity field in a horizontal domain. Simultaneous reciprocal transmissions of high frequency sound pulses were carried out for 9 hours along 16 ray paths. It is demonstrated that the application of this novel travel-time sensor (FAT) in conjunction with inversion schemes provides an effective tool to determine the depth-averaged currents magnitude in extremely shallow estuaries with complex flow distribution. To compare the tomographically derived results with those of a widely applied methods, round-trip moving-boat ADCP measurements were carried out every 30 min. It was found that, most of the time, section-averaged ADCP velocity data compares favorably with the corresponding inverse analysis results. Only during tide reversal period around high water, sound pulses are trapped in two conduits formed in the upper cold freshwater and lower warm seawater. As a result, FAT results are biased and inversion results deviates from those of moving-boat ADCP.
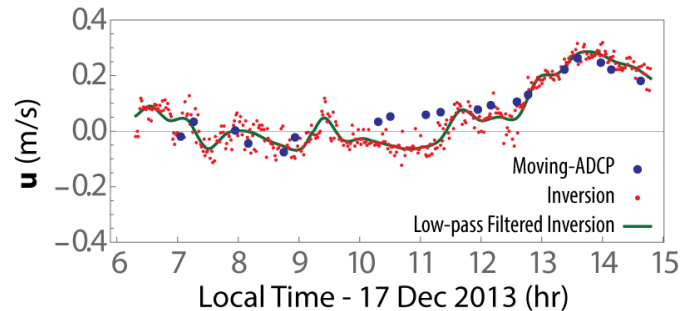

Figure 6. Comparison between section-averaged velocities measured by the moving-ADCP and obtained from inversion. The solid line denotes data passed through a low-pass filter with 30 min cut-off.

REFERENCES

Kaneko, A., Yuan, G., Gohda, N., Nakano, I., 1994. Optimum design of the ocean acoustic tomography system for the Sea of Japan. Journal of Oceanography 50, 281-293.

Kawanisi, K., Razaz, M., Kaneko, A., Watanabe, S., 2010. Long-term measurement of stream flow and salinity in a tidal river by the use of the fluvial acoustic tomography system. J Hydrol 380, 74-81.

Medwin, H., 1975. Speed of Sound in Water - Simple Equation for Realistic Parameters. J Acoust Soc Am 58, 1318-1319.

Munk, W., Worcester, P., Wunsch, C., 1995. Ocean acoustic tomography. Cambridge University Press, Cambridge ; New York.

Razaz, M., Kawanisi, K., Kaneko, A., Nistor, I., 2016. Application of acoustic tomography to reconstruct the horizontal flow velocity field in a shallow river. Water Resour Res.

Razaz, M., Kawanisi, K., Nistor, I., Sharifi, S., 2013. An acoustic travel time method for continuous velocity monitoring in shallow tidal streams. Water Resour Res 49, 4885-4899.

Simon, M.K., Omura, J.K., Levitt, B.K., 1985. Spread Spectrum Communications Handbook. McGraw-Hill, New York.